The Hippo kinase cascade regulates a contractile cell behavior and cell density in a close unicellular relative of animals

Authors:

Jonathan E Phillips, Duojia Pan*

Affiliation:

Department of Physiology, Howard Hughes Medical Institute, University of Texas Southwestern Medical Center, Dallas, Texas 75390, USA

* correspondence: duojia.pan@utsouthwestern.edu

ABSTRACT

The genomes of close unicellular relatives of animals encode orthologs of many genes that regulate animal development. However, little is known about the function of such genes in unicellular organisms or the evolutionary process by which these genes came to function in multicellular development. The Hippo pathway, which regulates cell proliferation and tissue size in animals, is present in some of the closest unicellular relatives of animals, including the amoeboid organism *Capsaspora owczarzaki*. We previously showed that the *Capsaspora* ortholog of the Hippo pathway nuclear effector Yorkie/YAP/TAZ (coYki) regulates actin dynamics and the three-dimensional morphology of *Capsaspora* cell aggregates, but is dispensable for cell proliferation control (Phillips et al., 2022). However, the function of upstream Hippo pathway components, and whether and how they regulate coYki in *Capsaspora*, remained unknown. Here, we analyze the function of the upstream Hippo pathway kinases coHpo and coWts in *Capsaspora* by generating mutant lines for each gene. Loss of either kinase results in increased nuclear localization of coYki, indicating an ancient, premetazoan origin of this Hippo pathway regulatory mechanism. Strikingly, we find that loss of either kinase causes a contractile cell behavior and increased density of cell packing within *Capsaspora* aggregates. We further show that this increased cell density is not due to differences in proliferation, but rather actomyosin-dependent changes in the multicellular architecture of aggregates. Given its well-established role in cell density-regulated proliferation in animals, the increased density of cell packing in *coHpo* and *coWts* mutants suggests a shared and possibly ancient and conserved function of the Hippo pathway in cell density control. Together, these results implicate cytoskeletal regulation but not proliferation as an ancestral function of the Hippo pathway and uncover a novel role for Hippo signaling in regulating cell density in a proliferation-independent manner.

INTRODUCTION

Despite the increasing recognition that the last unicellular ancestor of animals possessed many genetic components that mediate development in modern animals (Ros-Rocher et al., 2021), little is known about the function of such developmental regulators in the unicellular ancestor, and the process of how such genes came to function in these roles over evolutionary time is poorly understood. One example of a developmental pathway that is now known to be conserved in close unicellular relatives of animals is the Hippo pathway, which regulates tissue size in animals (Zheng and Pan, 2019). The Hippo pathway consists of a kinase cascade in which the kinase Hippo/MST phosphorylates the kinase Warts/LATS, which in turn phosphorylates the transcriptional coactivator Yorkie/YAP/TAZ, resulting in inactivation though cytoplasmic sequestration (Figure 1A, (Ma et al., 2019)). In the nucleus, Yorkie/YAP/TAZ forms a complex with the transcription factor Sd/TEAD, and this complex drives the expression of genes that promote proliferation and affect cell differentiation (Wu et al., 2008). The Hippo pathway thus serves to inhibit Yorkie/YAP/TAZ activity, and by this regulatory activity restricts tissue growth in development and homeostasis. In cultured cells, the Hippo pathway is known to be regulated by cell density in a process called contact inhibition, whereby Hippo signaling is low in sparse culture to allow cell proliferation but activated in confluent culture to arrest proliferation (Zhao et al., 2007). Although the state of the cytoskeleton (Dupont et al., 2011) and epithelial cell architecture (Yang et al., 2015) are known to regulate Hippo signaling, and many additional upstream regulatory components have been identified (Deng et al., 2015; Hamaratoglu et al., 2006; Yu et al., 2010; Zheng et al., 2017), how exactly Hippo signaling is regulated to achieve appropriate tissue size during development or stop cell proliferation in confluent cultures remains incompletely understood. As Hippo pathway dysregulation underlies multiple human cancer types (Zanconato et al., 2016), a more complete understanding of Hippo pathway regulation could guide the development of novel cancer therapeutics.

Although once thought to be present only in animals, the Hippo pathway is now known to be present in some of the closest unicellular relatives of animals (Figure 1B, (Sebe-Pedros et al., 2012)). One such unicellular organism is *Capsaspora owczarzaki* from the clade Filasterea, the sister group to Choanozoa (a clade comprising animals and choanoflagellates) (Shalchian-Tabrizi et al., 2008). *Capsaspora* is a motile amoeboid organism with a 5-micron-diameter cell body covered with F-actin-rich microvilli-like structures, and was initially identified as an apparent endosymbiont in the snail *B. glabrata (Stibbs et al., 1979)*. However, all other known filasterians

are apparent free-living heterotrophs (Hehenberger et al., 2017; Patterson et al., 1993; Tong, 1997), and whether *Capsaspora* is an obligate or facultative endosymbiont is not known. Physical or chemical signals can induce *Capsaspora* cells to aggregate into round, 3-dimensional multicellular structures that require calcium for cell-cell adhesion (Ros-Rocher et al., 2023; Sebe-Pedros et al., 2013). *Capsaspora* is easily culturable in axenic medium, has a complete genome with chromosome-level assembly (Schultz et al., 2023; Suga et al., 2013), and is genetically tractable owing to gene disruption and stable transgenic techniques that we have recently developed (Phillips et al., 2022). Further, the *Capsaspora* genome contains many genes once thought specific to animals, such as cell-cell adhesion and ECM proteins (cadherins, integrins, and laminins) and developmental regulators (NF-κB, P53/63/73, Brachyury, and RUNX) (Suga et al., 2013). Therefore, along with other emerging holozoan research organisms (Booth and King, 2020; Kozyczkowska et al., 2021; Olivetta and Dudin, 2023), *Capsaspora* is a valuable system for studying the function of such genes in unicellular organisms.

Previously, we have studied the role of the Hippo pathway in *Capsaspora* by generating a mutant of the single Yorkie/YAP/TAZ ortholog found in the genome (coYki) (Phillips et al., 2022). We found that coYki affects cytoskeletal dynamics, with coYki mutants showing constant ectopic blebbing at the cell cortex. Further, coYki affects the morphology of multicellular aggregates: whereas WT aggregates are spheroid, coYki mutant aggregates are flat and less circular than WT. Despite the well-characterized role of Yorkie/YAP/TAZ in promoting proliferation in animals, we saw no effect on cell proliferation in the coYki mutant, suggesting that regulation of proliferation by Yorkie/YAP/TAZ emerged after the last common ancestor of *Capsaspora* and animals. However, two important questions remain unanswered: 1) do the upstream components of the Hippo pathway regulate coYki, as they do in animals? 2) What effect does an increase of coYki activity have on *Capsaspora*?

In this study, we addressed these questions by generating homozygous mutant cell lines for the Hippo (coHpo) and Warts (coWts) kinases in *Capsaspora*. Loss of either kinase results in increased nuclear localization of coYki, showing that the regulatory activity of the Hippo kinase cascade is conserved. Loss of coHpo or coWts does not increase cell proliferation, consistent with our previous conclusion that the Hippo pathway does not significantly affect proliferation in *Capsaspora*. However, loss of either kinase results in a distinct cytoskeletal phenotype: cells display a contractile behavior in which an initially round cell will elongate on an axis, adhere to the substrate at two terminal adhesion sites connected by an F-actin fiber, and then undergo

contraction, returning to a round morphology. Further, we find that loss of these kinases increases the density of cell packing within multicellular aggregates, and we present evidence that this cell packing phenotype involves actomyosin-mediated contractile forces. Transgenic expression of a coYki mutant predicted to be hyperactive results in phenotypes like those observed in the coHpo and coWts mutants, suggesting that these phenotypes are caused by increased coYki activity due to a lack of kinase activity. Together, these results support our previous conclusions that the Hippo pathway regulates cytoskeletal dynamics but not proliferation in *Capsaspora*. In light of its well-established role in cell density-regulated proliferation control in animals, we speculate that the Hippo pathway may represent an ancient mechanism of cell density control preceding the emergence of animal multicellularity.

RESULTS

The Hippo pathway kinases regulate the subcellular localization of coYki in *Capsaspora*

Characterizing the function of the Hippo pathway in close unicellular relatives of animals may a) enhance our understanding of the evolutionary origins and ancestral function of this pathway and b) provide a relatively simple system to better understand how this biomedically significant pathway is regulated. To address these aims, we generated homozygous mutant cell lines for the single *Capsaspora* orthologs of the Hippo/MST and Warts/LATS kinases (coHpo and coWts, respectively.) For each gene, homologous recombination was used to replace the kinase domain of both WT alleles with selectable markers (Figure 1- figure supplement 1) as described previously (Phillips et al., 2022). Homozygous mutation of the kinases was verified by PCR and by sequencing the disrupted region of the genes (Figure 1- figure supplement 1).

In animals, the Hippo kinase cascade regulates the transcriptional coactivator Yorkie/YAP/TAZ by phosphorylation-mediated cytoplasmic sequestration (Dong et al., 2007). To test if the Hippo kinase cascade similarly regulates the subcellular localization of the single YAP/TAZ/Yorkie orthologue in *Capsaspora* (coYki), we transiently co-transfected WT, *coHpo-/-*, and *coWts-/-* cells with the fluorescent fusion proteins mScarlet-coYki and Histone H2B-Venus, a marker of the nucleus. In WT cells, mScarlet-coYki was predominantly cytoplasmic (Figure 1C), as reported previously (Phillips et al., 2022). In contrast, the majority of *coHpo-/-* and *coWts-/-* cells showed nuclear levels of mScarlet-coYki greater than or equal to that seen in the cytoplasm (Figure 1C and D). Interestingly, we found that *coWts-/-* cells were significantly more likely to show nuclear mScarlet-coYki localization than *coHpo-/-* cells (Figure 1D), which is consistent with Hpo/MST-independent activity of Wts/LATS previously reported in *Drosophila* and mammals (Zheng et al., 2015). Together, these results show that the *Capsaspora* Hippo kinase cascade regulates coYki by cytoplasmic sequestration, indicating a premetazoan origin of this regulatory activity of the Hippo pathway.

The Hippo pathway kinases do not restrict cell proliferation in *Capsaspora*

The Hippo pathway negatively regulates tissue size and cell proliferation by restricting the activity of the growth-promoting oncogene Yorkie/YAP/TAZ in animals. However, we have previously reported that *coYki* is genetically dispensable for cell proliferation in *Capsaspora* (Phillips et al.,

151 2022). To further evaluate the role of proliferation control by the Hippo pathway in *Capsaspora*,
152 we examined the requirement of *coHpo* and *coWts* in cell proliferation control under three distinct
153 conditions: adherent growth while attached to a solid substrate, proliferation in shaking culture,
154 and proliferation within multicellular aggregates. In adherent growth conditions, *coWts*-/- and
155 *coHpo*-/- cells proliferated at similar rates as WT cells (Figure 2A). In shaking culture, *coHpo-/-*
156 cells proliferated at similar rates as WT cells, whereas *coWts-/-* cells proliferated slower than WT
157 (Figure 2B). As cells lacking a negative regulator of proliferation are expected to proliferate faster
158 than WT cells, this result suggests that coWts is not a negative regulator of cell proliferation as in
159 *Drosophila* and mammals, but instead is required for normal cell viability under some growth
160 conditions. Finally, to examine cell proliferation within multicellular aggregates, we used EdU
161 labeling, a marker of cells that have undergone S phase. The percentage of cells labeled by EdU
162 in *coHpo-/-* and *coWts-/-* aggregates was not significantly different from WT aggregates (Figure
163 2C and D), indicating that coHpo and coWts do not affect cell proliferation within multicellular
164 aggregates. Together with our previous characterization of *coYki* (Phillips et al., 2022), these
165 results support the view that the Hippo pathway kinases coHpo and coWts do not restrict cell
166 proliferation in *Capsaspora* as in *Drosophila* and mammals.
167
168 **The Hippo pathway kinases regulate cell morphology and actomyosin-dependent**
169 **contractile behaviors in *Capsaspora***
170
171 We have previously shown that, in contrast to WT *Capsaspora* cells with a round and relatively
172 stable actin cortex, *coYki-/-* cells show aberrant, actin-depleted bleb-like protrusions at the cell
173 cortex, implicating coYki in the control of cytoskeletal dynamics and cell morphology (Phillips et
174 al., 2022). To test whether the Hippo pathway kinases affect the same processes in *Capsaspora,*
175 we examined the morphology of adherent *coHpo-/-* and *coWts-/-* cells. While most cells showed
176 a round cell body morphology (Figure 3A), a distinct elongated cell morphology was observed in
177 a subset of *coWts* -/- or *coHpo* -/- cells, which was seen much less frequently in WT cells.
178 Quantification of cellular aspect ratio in cell populations showed a non-gaussian distribution, with
179 a distinct population of high aspect ratio cells in *coHpo* or *coWts* mutants (Figure 3B). The
180 presence of elongated cells was rescued by transgenic expression of coHpo or coWts in the
181 respective mutant (Figure 3A and B), demonstrating that the elongated cell phenotype was
182 specifically due to the absence of these kinases.
183

184 To examine the dynamic properties of these elongated cells, we imaged *coHpo -/-* and *coWts -/-*
185 cells by time-lapse microscopy (Figure 3C and Videos S1-S3). These elongated cells are highly
186 dynamic. A previously round, motile cell starts extending along an axis, the direction of which
187 does not necessarily correspond with the cell's previous direction of movement. The cell then
188 stops extending, remaining for approximately 20 seconds in its elongated form. Microvilli appear
189 enriched at the poles of elongated cells (Figure 3C, 2:00 timepoint), although it is not clear whether
190 more microvilli are present at the poles, or whether microvilli at the poles are more adherent to
191 the substrate and are thus more visible microscopically. After this elongated form, the cell then
192 contracts: adhesion at one of the poles is apparently lost, leading to a rapid contractile movement
193 toward the other pole and returning the cell to the initial round morphology. Together, these results
194 suggest that *Capsaspora* cells can perform a dynamic contractile behavior that is regulated by
195 the Hippo pathway kinases.
196
197 The actomyosin cytoskeletal network mediates amoeboid motion and cytokinesis in unicellular
198 organisms and contractile processes such as muscle contraction in animals (Brunet and Arendt,
199 2016). To examine the behavior of the actomyosin network in contractile *Capsaspora* cells, we
200 stably expressed Lifeact-mScarlet, which labels F-actin in *Capsaspora* cells (Phillips et al., 2022).
201 As contractile cells in the *coHpo* mutant background tended to show a more extreme elongated
202 morphology than the *coWts* mutant, we focused on the *coHpo* mutant for further analysis. We
203 have previously reported that adherent WT *Capsaspora* cells show F-actin-rich foci near the area
204 of contact with the substrate. In motile cells, these foci do not move relative to the substrate,
205 suggesting that they are points of adhesion (Phillips et al., 2022). Similar F-actin-rich foci were
206 observed at or near the polar ends of elongated *coHpo -/-* cells (Figure 4A, blue arrowheads). In
207 most elongated cells, an F-actin fiber running parallel to the axis of elongation was observed
208 connecting the two polar foci (Figure 4A, yellow arrow; Videos S4-S5). During the contractile
209 process, the cell contracts towards one of the foci, which remains intact, while the other substrate-
210 foci interaction is lost, and the cell resumes a round morphology.
211
212 Superficially, the actin fibers observed in elongated *coHpo -/-* cells resemble stress fibers, which
213 are contractile cytoskeletal structures found in animal cells with functions in processes such as
214 extracellular matrix remodeling and cell motility (Tojkander et al., 2012). Contractility of stress
215 fibers is generated by the motor protein myosin II (Chrzanowska-Wodnicka and Burridge, 1996).
216 If myosin mediates the contractile behavior of *coHpo -/-* cells, then inhibition of myosin activity
217 may slow or prevent the contraction of elongated cells, resulting in more cells with an elongated

218 morphology in a population. To test this prediction, we treated cells with the myosin inhibitor
219 blebbistatin and then examined the occurrence of elongated cell morphology. Blebbistatin
220 treatment increased the occurrence of elongated cell morphology in *coHpo -/-* cell populations
221 (Figure 4B and C). Interestingly, despite the rarity of elongated cell morphology in WT cell
222 populations, blebbistatin also resulted in greatly increased occurrence of this morphology in WT
223 cell populations. (Figure 4B and C). These results suggest that the contractile behavior of
224 *Capsaspora* cells is mediated by myosin activity.
225
226 **The Hippo pathway kinases regulate the density of cell packing in *Capsaspora* aggregates**
227 **via actomyosin-mediated contractility**
228
229 *Capsaspora* cells can aggregate into three-dimensional multicellular structures. We have
230 previously identified a critical role for coYki in this process: whereas WT *Capsaspora* cells form
231 round, spheroid aggregates, *coYki-/-* cells form asymmetrical and flattened aggregates (Phillips
232 et al., 2022). To test whether the Hippo pathway kinases regulate aggregate morphology, we
233 induced aggregate formation and then measured the size and circularity of aggregates. *coHpo -*
234 */-* aggregates showed similar size and circularity as WT aggregates (Figure 5A and B). However,
235 *coWts -/-* aggregates, while similar in size to WT, showed reduced circularity. Whereas WT
236 aggregates showed a round, smooth boundary, *coWts -/-* aggregate boundaries were rough and
237 showed nonuniform protrusions (Figure 5A and B). These results suggest that Hippo signaling
238 through coWts can affect aggregate morphology, but inactivation of the upstream Hippo kinase
239 alone is not sufficient to induce this effect.
240
241 *Capsaspora* aggregates are composed of adherent cells that form connections primarily through
242 microvilli-like protrusions on the cell surface. This can be visualized by mosaic aggregates
243 consisting of cells expressing mScarlet, which labels the cell body, and cells expressing NMM-
244 Venus, which labels the cell membrane and allows visualization of the microvilli (Parra-Acero et
245 al., 2018). In mosaic aggregates, contacts are visible between microvilli but not between cell
246 bodies (Figure 5C), showing that microvilli-microvilli contacts, but not cell body to cell body
247 contacts, are the primary mode of adhesion in aggregates.
248
249 While examining aggregate morphology by, we noticed that *coHpo -/-* aggregates appeared more
250 opaque than WT, suggesting that the Hippo pathway kinases may affect the internal structure of
251 aggregates. To investigate this further, we stably expressed mScarlet in WT, *coHpo -/-*, *coWts -/-*

252 , and *coYki -/-* cells and then used optical sectioning to examine aggregate inner structure. This
253 analysis revealed that cells within *coHpo -/-* or *coWts -/-* aggregates appeared more tightly packed
254 than WT (Figure 5D). To quantify this effect, we measured the number of cells per unit area in
255 optical sections of aggregates. Whereas the number of cells per unit area in *coYki -/-* aggregates
256 was not significantly different from WT, the number of cells per area in *coHpo -/-* and *coWts -/-*
257 was significantly increased relative to WT (Figure 5E). These results indicate that loss of the Hippo
258 pathway kinases increases cell packing within *Capsaspora* aggregates.
259
260 Given that *coHpo* and *coWts* regulate a contractile behavior in *Capsaspora* cells, a plausible
261 explanation for the increased cell packing within *coHpo -/-* and *coWts -/-* aggregates is that an
262 increase in intercellular contractile interactions pulls cells closer and therefore leads to increased
263 cell density in mutant aggregates. To test whether actomyosin-mediated contractile forces affect
264 cell packing within aggregates, we treated WT and *coHpo -/-* aggregates with the myosin II
265 inhibitor blebbistatin or the actin-depolymerizing drug latrunculin B (LatB). For both WT and *coHpo*
266 *-/-* aggregates, treatment with either blebbistatin or LatB decreased cell density within aggregates,
267 as reflected by a reduction in the number of cells per unit area (Figure 6A-D). Together, these
268 results suggest that the Hippo pathway kinases regulate the density of cell packing in *Capsaspora*
269 aggregates via actomyosin-mediated contractility .
270
271 *coYki* affects both the cytoskeletal dynamics of *Capsaspora* cells and the shape of multicellular
272 aggregates (Phillips et al., 2022). Given these previous results and the fact that Yorkie/YAP/TAZ
273 is inhibited by the Hippo pathway kinases in other organisms, it is plausible that the phenotypes
274 observed in the *coHpo* and *coWts* mutants are mediated by *coYki.* Since techniques are currently
275 unavailable to create double mutants in *Capsaspora*, we could not test this possibility through
276 classic genetic epistasis. As an alternative approach, we asked whether ectopic activation of
277 *coYki* can phenocopy the loss of *coHpo* or *coWts*, by transgenically expressing a coYki mutant in
278 which the four predicted Wts/LATS phosphorylation sites are mutated to non-phosphorylatable
279 Alanine (coYki 4SA). coYki 4SA shows increased nuclear localization compared to the wild-type
280 coYki protein (Phillips et al., 2022), and thus is predicted to be hyperactive. As observed in *coHpo*
281 and *coWts* mutants, stable transgenic expression of coYki 4SA resulted in increased cell packing
282 of *Capsaspora* aggregates (Figure 7 A and B), as well as an elongated cell morphology in
283 adherent cells (Figure 7 C and D). These results suggest that the phenotypes observed in *coHpo*
284 and *coWts* mutants are due to coYki activation resulting from a loss of upstream kinase signaling.
285

Discussion

The evolutionary process by which the signaling pathways that regulate animal development came to function in these roles remains unclear. Apart from shedding light on the origin of animals, knowledge about this process could provide a deeper understanding of these signaling pathways, which play key roles in human health and disease. Although we cannot study the ancestral unicellular organisms that gave rise to animals, studying modern close unicellular relatives of animals can guide our understanding of what these organisms may have been like, and how conserved signaling pathways may have functioned in these unicellular ancestors. Our previous characterization of the Yorkie/YAP/TAZ ortholog coYki in *Capsaspora* showed that coYki affects actin dynamics and the shape of multicellular aggregates in this close unicellular relative of animals. However, we saw no effect on proliferation in the coYki mutant, suggesting that regulation of proliferation by Yorkie/YAP/TAZ may have evolved later in the lineage leading to animals. In this report, we build on our previous study by assessing the function of the upstream kinases coHpo and coWts in *Capsaspora*. We find that the mechanism of Yorkie/YAP/TAZ regulation (specifically, cytoplasmic sequestration by upstream kinase activity) is conserved in *Capsaspora* and animals, indicating an ancient origin of this signaling machinery. These findings support and extend our previous study uncovering a role for Hippo signaling in the regulation of cytoskeletal dynamics but not cell proliferation. Together, our studies suggest that the ancestral function of the Hippo pathway was cytoskeletal regulation, and that subsequently the pathway was co-opted to regulate cell proliferation and tissue size in animals.

In this report, we describe a contractile cell behavior observed in *coHpo* and *coWts* mutants. In this process, the cell transitions from a round morphology to an elongated spindle shape. The cell will remain in the spindle shape for approximately 20 seconds and then contract towards one pole. We interpret this as a process in which cells extend and then adhere to the substrate at the two ends of the spindle, contractile forces within the cell increase, and adhesion at one of the poles is subsequently lost, leading to contraction towards the other pole. Visualization of actin in live cells is consistent with this model: we observed actin-rich foci at the adhesive sites at the poles of spindle-shaped cells, and an actin filament connecting these foci, which may serve as a tension-generating structure. The cytoskeletal structures that we observe resemble adhesive/contractile structures in mammalian cells such as podosomes (Linder et al., 2023), focal adhesions (Fierro Morales et al., 2022), and stress fibers (Tojkander et al., 2012). As *Capsaspora* encodes orthologs of some proteins known to label these structures, future colocalization

experiments may reveal the degree of conservation between such subcellular structures in *Capsaspora* and animals.

The function of these contractile cells is presently unclear. While we observed the contractile behavior on glass surface, which is likely non-physiological, we speculate that such contraction exerted on a pliable surface may remodel a cell's extracellular environment to provide certain fitness benefits. Intriguingly, the elongated, spindle morphology was reported to be common (nearly 50 percent of cells) after isolation of *Capsaspora* cells from the *B. glabrata* snail host (Stibbs et al., 1979), suggesting that environmental factors from the snail host may affect this elongated morphology and potentially Hippo pathway signaling. We further speculate that increased contractility within multicellular aggregates may serve to pull the neighboring cells closer to each other, which may contribute to the increased packing in the of *coHpo* or *coWts* mutant aggregates.

We show that the elongated cell morphology visible in *coHpo* and *coWts* mutants becomes more common after treatment with blebbistatin, indicating a role for myosin II in the contraction of this elongated cell state. One interpretation of the increase in elongated cells in the *coHpo* and *coWts* mutants, therefore, is that myosin activity is reduced. However, we also see that blebbistatin treatment reduces the packing of cells within multicellular groups, whereas loss of *coHpo* or *coWts* causes an increase in cell packing. Thus the specific role of myosin activity in the phenotypes observed in Hippo pathway mutants in *Capsaspora* remains unclear. One possibility is that the initial process of cell elongation is unrelated to myosin, and it is this process that is enhanced in *coHpo* and *coWts* mutants. Although techniques to visualize and quantify myosin activity in *Capsaspora* have not been developed, future work in this regard could elucidate the relationship between myosin activity and Hippo signaling in *Capsaspora.*

Previous work has examined the structure of *Capsaspora* aggregates by electron microscopy (Sebe-Pedros et al., 2013). In this report we have furthered our understanding of aggregate structure by providing evidence that a) cells within aggregates appear to contact their neighbors largely by interactions between microvilli; and b) Hippo pathway activity affects the packing of cells within these aggregates. In animals, the predominant form of multicellular structure is epithelia, in which cells with apical-basal polarity form lateral contacts at adherens junctions, septate junctions, tight junctions, and desmosomes (Abedin and King, 2010). However, microvilli/filopodial adhesion plays important roles in dorsal closure in *Drosophila* (Jacinto et al.,

2000), early embryo compaction in mouse (Fierro-Gonzalez et al., 2013), and other developmental processes (Brunet and Booth, 2023). Further, inter-microvillar contacts are the apparent means of adherence in the choanoflagellate *C. flexa,* another close unicellular relative of animals, that can exist in a sheet-like morphology with a remarkable actomyosin-dependent inverting activity (Brunet et al., 2019). Thus microvilli-mediated adhesion may be an ancient and conserved means of multicellularity that preceded the formation of epithelia.

In cultured mammalian cells, Hippo signaling regulates contact inhibition, a phenomenon in which proliferation is arrested upon cell confluency to achieve a proper cell density (Aragona et al., 2013; Zhao et al., 2007). Interestingly, while Hippo signaling does not regulate cell proliferation in *Capsaspora*, loss of Hippo pathway kinases or increase in coYki activity increases the density of cell packing within *Capsaspora* aggregates. Thus, despite the distinct routes of achieving proper cell density (cell proliferation vs. cell aggregation), the Hippo pathway appears to restrict cell density in both animals and *Capsaspora*. We speculate that the Hippo pathway may represent an ancient mechanism of cell density control preceding the emergence of animal multicellularity. Significantly, this model suggests that the signals that regulate the Hippo pathway in animals and *Capsaspora* may be conserved, and therefore studying *Capsaspora* could provide important insights into the regulation of this biomedically significant pathway.

373 **MATERIALS AND METHODS**

374

Key Resources Table				
Reagent type (species) or resource	**Designation**	**Source or reference**	**Identifiers**	**Additional information**
gene (*Capsaspora owczarzaki*)	*coHpo*	Genbank	CAOG_01932	
gene (*Capsaspora owczarzaki*)	*coWts*	Genbank	CAOG_00619	
gene (*Capsaspora owczarzaki*)	*coYki*	Genbank	CAOG_07866	
cell line (*Capsaspora owczarzaki*)	WT	ATCC	30864	
recombinant DNA reagent	pJP80	(Phillips et al., 2022)		*Capsaspora* expression vector: mScarlet-coYki fusion, Geneticin resistance
recombinant DNA reagent	pONSY-coH2B:Venus	Addgene	Addgene Plasmid #111877	*Capsaspora* expression vector: Histone H2B-Venus fusion
recombinant DNA reagent	pJP122	This paper		*Capsaspora* expression vector: coHpo transgene, Hygromycin B Resistance
recombinant DNA reagent	pJP125	This paper		*Capsaspora* expression vector: coWts transgene, Hygromycin B Resistance
recombinant DNA reagent	pJP145	This paper		*Capsaspora* expression vector: NMM-Venus, Hygromycin B Resistance

recombinant DNA reagent	pJP118	(Phillips et al., 2022)		*Capsaspora* expression vector: Lifeact-mScarlet, Hygromycin B Resistance
recombinant DNA reagent	pJP103	(Phillips et al., 2022)		*Capsaspora* expression vector: mScarlet, Hygromycin B Resistance
recombinant DNA reagent	pJP90	(Phillips et al., 2022)		*Capsaspora* expression vector: coYki 4SA , Geneticin Resistance
sequence-based reagent	oJP201: coHpo KO Forward: homologous arm + actin promoter	This paper	PCR primers	CCCGCCTCGTCCCAACAAC AGCTCGTACGGCTCGGTCT TCAAGGCTCGCCACAAGGA CACCCAGTCCATCCTCGCC GTCAAGCAGGTGCCCCTTG AGAAC**ACAAAAATGCTGAT TGTTTG**
sequence-based reagent	oJP202: coHpo KO Reverse: homologous arm + actin terminator	This paper	PCR primers	AAGCAACATTGCTTCGTTG ACTAACGCTTCATGGTGCC GTCCTCGCCCATGACCATC GTGCCGGAGTCGCCAGTG ACCATCGTTCCGCTATCAA CAAGGG**TTTTTTCTTTGTAC AAGATCAC**
sequence-based reagent	oJP203: coWts KO Forward: homologous arm + actin promoter	This paper	PCR primers	CAAACGGCGAGACCAGCT CGAGATTGAGATGGCCAAG ATGGACCTGACCGATGTTC AAAAGACCCAGTTGCGTCG CATCCTCCGCATGAAGGAA TCAGAG**ACAAAAATGCTGA TTGTTTG**
sequence-based reagent	oJP204: coWts KO Reverse: homologous arm + actin terminator	This paper	PCR primers	GCATTTTAATGTGCTCGAC CGTCTCCCGGCCGAGACG ATCGGAGGATTCACAGCAG AGCCGGGAGATGAGGTCTT TGGACTCGCGCGAAATCTT TGCCCG**TTTTTTCTTTGTAC AAGATCAC**
sequence-based reagent	oJP205: coHpo Diagnostic Forward	This paper	PCR primers	CAAAAACAACAGCGAAAAC G

sequence-based reagent	oJP206: coHpo Diagnostic Reverse	This paper	PCR primers	CCATCGGAGGAAACTAAAGG
sequence-based reagent	oJP207: coWts Diagnostic Forward	This paper	PCR primers	TGCTGCTGAAAATGAAAACG
sequence-based reagent	oJP208: coWts Diagnostic Reverse	This paper	PCR primers	GAACCTCACCAGGATTTTGC
commercial assay or kit	TransIT-X2 Dynamic Delivery System	Mirus Bio	MIR 6003	
commercial assay or kit	Click-iT™ Plus EdU Cell Proliferation Kit for Imaging, Alexa Fluor™ 488 dye	ThermoFisher	C10637	
chemical compound, drug	Blebbistatin	Sigma-Aldrich	B0560	
chemical compound, drug	Latrunculin B	Sigma-Aldrich	L5288	

375
376
377

378 Cell culture

379 *Capsaspora* cells were grown in ATCC medium 1034 as described previously (Phillips et al.,
380 2022). Quantification of proliferation in shaking culture, induction of aggregates, quantification of
381 aggregate size and circularity, EdU labeling within aggregates, and quantification of mScarlet-
382 coYki fluorescence intensity were done as described previously (Phillips et al., 2022).
383 Quantification of proliferation on a solid substrate was done as described previously (Phillips et
384 al., 2022), except 96-well plates were used in place of 24-well plates. To add blebbistatin (Sigma
385 B0560) or latrunculin B (Sigma L5288) to cell cultures, a 10X mix of drug or vehicle control in
386 growth medium was prepared, and this concentrated drug preparation was added to cultures so
387 that a final 1X concentration of drugs was reached.

388

389 Molecular Biology

390 For a list of plasmids and oligonucleotides generated for this study, see Key Resources Table.
391 For a list of synthesized DNA sequences used in this study, see Supplemental Data S1. For
392 transgenic expression of *Capsaspora* genes, we synthesized genes coding for the appropriate
393 *Capsaspora* protein but with synonymous codon changes throughout the DNA sequence. This
394 was done to reduce DNA sequence homology in order to prevent homologous recombination of
395 the transgene with the endogenous *Capsaspora* alleles during plasmid integration into the
396 genome, as done previously (Phillips et al., 2022). To construct a plasmid for transgenic
397 expression of coHpo in *Capsaspora* cells (pJP122), we synthesized a transgene encoding the
398 coHpo protein (sJP201). There are three predicted isoforms of the coHpo sequence, but only one
399 of these encodes the SARAH domain, which is important for Hippo kinase activity in Hippo
400 pathway signaling (Scheel and Hofmann, 2003). We therefore used the isoform sequence
401 encoding the SARAH domain to design our transgene. The coHpo transgene was cloned into a
402 KpnI and AflII digest of pJP103 (Addgene #176481) using Gibson assembly, generating a vector
403 encoding the coHpo transgene and hygromycin B resistance. Similarly, a coWts transgene was
404 synthesized (sJP202) and cloned into a KpnI and AflII digest of pJP103 by Gibson assembly,
405 generating a vector encoding a coWts transgene and hygromycin B resistance (pJP125.)

406

407 To generate a plasmid to stably express N-myristoylation motif (NMM)-Venus (pJP145), a marker
408 of the plasma membrane and microvilli in *Capsaspora*, we first constructed a vector expressing
409 both Venus and hygromycin B resistance (pJP115) by PCR-amplifying the Venus gene from
410 pJP114 (Phillips et al., 2022) and cloning it by Gibson assembly into a KpnI and AflII digest of
411 pJP103 (Addgene #176481), which contains a hygromycin B resistance cassette. We then

412 synthesized the NMM motif (sJP203) following the sequence from the pONSY-coNMM:mCherry
413 vector (Addgene #111878, (Parra-Acero et al., 2018)) and cloned this DNA fragment into a KpnI
414 digest of pJP115 using Gibson assembly.
415
416 *Capsaspora* transfection and genome editing
417 Transfection of *Capsaspora* cells and stable cell line generation was done using the *Trans*IT-X2
418 transfection reagent (Mirus Bio) as previously described (Phillips et al., 2022). Disruptions of
419 *Capsaspora* genes were done as previously described (Phillips et al., 2022). Briefly, oligos
420 oJP201 and oJP202 were used to generate gene targeting constructs by PCR with homologous
421 arms that target the coHpo gene (CAOG_01932). Oligos oJP203 and oJP204 were used to
422 generate gene-targeting constructs for the coWts gene (CAOG_00619). For both homozygous
423 mutants, the two WT alleles present in the diploid *Capsaspora* genome were disrupted using
424 selectable markers for geneticin resistance and nourseothricin resistance. oJP205 and oJP206
425 were used in a diagnostic PCR that amplifies across the deleted region of the *coHpo* gene, and
426 oligos oJP207 and oJP208 were used in a diagnostic PCR across the deleted region of the *coWts*
427 gene.
428
429 Measurement of cell and aggregate properties
430 To measure the aspect ratio of cells, the ImageJ freehand selection tool was used to manually
431 trace the border of imaged cells, and the Measure function was used to calculate the cellular
432 aspect ratio. To quantify cell packing within aggregates expressing mScarlet, a z-stack of optical
433 sections was obtained by confocal microscopy. To measure cells within the aggregate as opposed
434 to cells at the edge of the aggregate, an optical section 14 microns deep into the aggregate was
435 used for measurement. A 40 micron^2 square was drawn in the center of the optical section of the
436 aggregate and the number of cells in the square was counted.
437
438 Gene nomenclature
439 In this article, we use italicized text to refer to a gene (e.g., *coHpo*), unitalicized text to refer to a
440 protein (e.g., coHpo), and '-/-' to indicate a homozygous deletion mutant (e.g., *coHpo -/-).* "*EF1 >*
441 *coHpo*" indicates transgenic expression of *coHpo* driven by the *EF1* promoter.
442
443 Statistics
444 Statistical analyses were done using Prism (GraphPad Software, San Diego, CA). For
445 experiments where multiple cells or aggregates were measured for each independent experiment,

446 the mean of all measurements made for each biological replicate was calculated, and statistical
447 analyses were performed on these sample level means following (Lord et al., 2020).
448
449 **Acknowledgements:**
450 We thank Maribel Santos for technical assistance with genotyping cell lines. We thank Dr. Iñaki
451 Ruiz-Trillo for the gift of pONSY-coH2B:Venus vector (Addgene plasmid number 111877). This
452 work was supported in part by National Institute of Health grant EY015708 to D.P. During this
453 work J.E.P was a Howard Hughes Medical Institute fellow of the Life Sciences Research
454 Foundation. D.P. is an investigator of the Howard Hughes Medical Institute.
455

456 **REFERENCES**

457

458 Abedin, M., and King, N. (2010). Diverse evolutionary paths to cell adhesion. Trends Cell Biol *20*,
459 734-742.

460 Aragona, M., Panciera, T., Manfrin, A., Giulitti, S., Michielin, F., Elvassore, N., Dupont, S., and
461 Piccolo, S. (2013). A Mechanical Checkpoint Controls Multicellular Growth through YAP/TAZ
462 Regulation by Actin-Processing Factors. Cell *154*, 1047-1059.

463 Booth, D.S., and King, N. (2020). Genome editing enables reverse genetics of multicellular
464 development in the choanoflagellate Salpingoeca rosetta. Elife *9*.

465 Brunet, T., and Arendt, D. (2016). From damage response to action potentials: early evolution of
466 neural and contractile modules in stem eukaryotes. Philos Trans R Soc Lond B Biol Sci *371*,
467 20150043.

468 Brunet, T., and Booth, D.S. (2023). Cell polarity in the protist-to-animal transition. Curr Top Dev
469 Biol *154*, 1-36.

470 Brunet, T., Larson, B.T., Linden, T.A., Vermeij, M.J.A., McDonald, K., and King, N. (2019). Light-
471 regulated collective contractility in a multicellular choanoflagellate. Science *366*, 326-334.

472 Chrzanowska-Wodnicka, M., and Burridge, K. (1996). Rho-stimulated contractility drives the
473 formation of stress fibers and focal adhesions. J Cell Biol *133*, 1403-1415.

474 Deng, H., Wang, W., Yu, J., Zheng, Y., Qing, Y., and Pan, D. (2015). Spectrin regulates Hippo
475 signaling by modulating cortical actomyosin activity. Elife *4*, e06567.

476 Dong, J., Feldmann, G., Huang, J., Wu, S., Zhang, N., Comerford, S.A., Gayyed, M.F., Anders,
477 R.A., Maitra, A., and Pan, D. (2007). Elucidation of a universal size-control mechanism in
478 Drosophila and mammals. Cell *130*, 1120-1133.

479 Dupont, S., Morsut, L., Aragona, M., Enzo, E., Giulitti, S., Cordenonsi, M., Zanconato, F., Le
480 Digabel, J., Forcato, M., Bicciato, S.*, et al.* (2011). Role of YAP/TAZ in mechanotransduction.
481 Nature *474*, 179-183.

482 Fierro Morales, J.C., Xue, Q., and Roh-Johnson, M. (2022). An evolutionary and physiological
483 perspective on cell-substrate adhesion machinery for cell migration. Front Cell Dev Biol *10*,
484 943606.

485 Fierro-Gonzalez, J.C., White, M.D., Silva, J.C., and Plachta, N. (2013). Cadherin-dependent
486 filopodia control preimplantation embryo compaction. Nat Cell Biol *15*, 1424-1433.

487 Hamaratoglu, F., Willecke, M., Kango-Singh, M., Nolo, R., Hyun, E., Tao, C., Jafar-Nejad, H., and
488 Halder, G. (2006). The tumour-suppressor genes NF2/Merlin and Expanded act through Hippo
489 signalling to regulate cell proliferation and apoptosis. Nat Cell Biol *8*, 27-36.

490 Hehenberger, E., Tikhonenkov, D.V., Kolisko, M., Del Campo, J., Esaulov, A.S., Mylnikov, A.P.,
491 and Keeling, P.J. (2017). Novel Predators Reshape Holozoan Phylogeny and Reveal the
492 Presence of a Two-Component Signaling System in the Ancestor of Animals. Curr Biol *27*, 2043-
493 2050 e2046.

494 Jacinto, A., Wood, W., Balayo, T., Turmaine, M., Martinez-Arias, A., and Martin, P. (2000).
495 Dynamic actin-based epithelial adhesion and cell matching during Drosophila dorsal closure.
496 Current Biology *10*, 1420-1426.

497 Kozyczkowska, A., Najle, S.R., Ocana-Pallares, E., Areste, C., Shabardina, V., Ara, P.S., Ruiz-
498 Trillo, I., and Casacuberta, E. (2021). Stable transfection in protist Corallochytriumlimacisporum
499 identifies novel cellular features among unicellular animals relatives. Curr Biol.

500 Linder, S., Cervero, P., Eddy, R., and Condeelis, J. (2023). Mechanisms and roles of podosomes
501 and invadopodia. Nat Rev Mol Cell Biol *24*, 86-106.

502 Lord, S.J., Velle, K.B., Mullins, R.D., and Fritz-Laylin, L.K. (2020). SuperPlots: Communicating
503 reproducibility and variability in cell biology. J Cell Biol *219*.

504 Ma, S., Meng, Z., Chen, R., and Guan, K.L. (2019). The Hippo Pathway: Biology and
505 Pathophysiology. Annu Rev Biochem *88*, 577-604.

506 Olivetta, M., and Dudin, O. (2023). The nuclear-to-cytoplasmic ratio drives cellularization in the
507 close animal relative Sphaeroforma arctica. Curr Biol *33*, 1597-1605 e1593.

508 Parra-Acero, H., Ros-Rocher, N., Perez-Posada, A., Kozyczkowska, A., Sanchez-Pons, N.,
509 Nakata, A., Suga, H., Najle, S.R., and Ruiz-Trillo, I. (2018). Transfection of Capsaspora
510 owczarzaki, a close unicellular relative of animals. Development *145*.

511 Patterson, D.J., Nygaard, K., Steinberg, G., and Turley, C.M. (1993). Heterotrophic Flagellates
512 and Other Protists Associated with Oceanic Detritus Throughout the Water Column in the Mid
513 North-Atlantic. J Mar Biol Assoc Uk *73*, 67-95.

514 Phillips, J.E., Santos, M., Konchwala, M., Xing, C., and Pan, D. (2022). Genome editing in the
515 unicellular holozoan Capsaspora owczarzaki suggests a premetazoan role for the Hippo pathway
516 in multicellular morphogenesis. Elife *11*.

517 Ros-Rocher, N., Kidner, R.Q., Gerdt, C., Davidson, W.S., Ruiz-Trillo, I., and Gerdt, J.P. (2023).
518 Chemical factors induce aggregative multicellularity in a close unicellular relative of animals. Proc
519 Natl Acad Sci U S A *120*, e2216668120.

520 Ros-Rocher, N., Perez-Posada, A., Leger, M.M., and Ruiz-Trillo, I. (2021). The origin of animals:
521 an ancestral reconstruction of the unicellular-to-multicellular transition. Open Biol *11*, 200359.

522 Scheel, H., and Hofmann, K. (2003). A novel interaction motif, SARAH, connects three classes of
523 tumor suppressor. Curr Biol *13*, R899-900.

524 Schultz, D.T., Haddock, S.H.D., Bredeson, J.V., Green, R.E., Simakov, O., and Rokhsar, D.S.
525 (2023). Ancient gene linkages support ctenophores as sister to other animals. Nature *618*, 110-
526 117.

527 Sebe-Pedros, A., Irimia, M., Del Campo, J., Parra-Acero, H., Russ, C., Nusbaum, C., Blencowe,
528 B.J., and Ruiz-Trillo, I. (2013). Regulated aggregative multicellularity in a close unicellular relative
529 of metazoa. Elife *2*, e01287.

530 Sebe-Pedros, A., Zheng, Y., Ruiz-Trillo, I., and Pan, D. (2012). Premetazoan origin of the hippo
531 signaling pathway. Cell Rep *1*, 13-20.

532 Shalchian-Tabrizi, K., Minge, M.A., Espelund, M., Orr, R., Ruden, T., Jakobsen, K.S., and
533 Cavalier-Smith, T. (2008). Multigene phylogeny of choanozoa and the origin of animals. PLoS
534 One *3*, e2098.

535 Stibbs, H.H., Owczarzak, A., Bayne, C.J., and DeWan, P. (1979). Schistosome sporocyst-killing
536 Amoebae isolated from Biomphalaria glabrata. J Invertebr Pathol *33*, 159-170.

537 Suga, H., Chen, Z., de Mendoza, A., Sebe-Pedros, A., Brown, M.W., Kramer, E., Carr, M., Kerner,
538 P., Vervoort, M., Sanchez-Pons, N.*, et al.* (2013). The Capsaspora genome reveals a complex
539 unicellular prehistory of animals. Nat Commun *4*, 2325.

540 Tojkander, S., Gateva, G., and Lappalainen, P. (2012). Actin stress fibers--assembly, dynamics
541 and biological roles. J Cell Sci *125*, 1855-1864.

542 Tong, S.M. (1997). Heterotrophic flagellates and other protists from Southampton Water, UK.
543 Ophelia *47*, 71-131.

544 Wu, S., Liu, Y., Zheng, Y., Dong, J., and Pan, D. (2008). The TEAD/TEF family protein Scalloped
545 mediates transcriptional output of the Hippo growth-regulatory pathway. Dev Cell *14*, 388-398.

546 Yang, C.C., Graves, H.K., Moya, I.M., Tao, C., Hamaratoglu, F., Gladden, A.B., and Halder, G.
547 (2015). Differential regulation of the Hippo pathway by adherens junctions and apical-basal cell
548 polarity modules. Proc Natl Acad Sci U S A *112*, 1785-1790.

549 Yu, J., Zheng, Y., Dong, J., Klusza, S., Deng, W.M., and Pan, D. (2010). Kibra functions as a
550 tumor suppressor protein that regulates Hippo signaling in conjunction with Merlin and Expanded.
551 Dev Cell *18*, 288-299.

552 Zanconato, F., Cordenonsi, M., and Piccolo, S. (2016). YAP/TAZ at the Roots of Cancer. Cancer
553 Cell *29*, 783-803.

554 Zhao, B., Wei, X., Li, W., Udan, R.S., Yang, Q., Kim, J., Xie, J., Ikenoue, T., Yu, J., Li, L.*, et al.*
555 (2007). Inactivation of YAP oncoprotein by the Hippo pathway is involved in cell contact inhibition
556 and tissue growth control. Genes Dev *21*, 2747-2761.

557 Zheng, Y., Liu, B., Wang, L., Lei, H., Pulgar Prieto, K.D., and Pan, D. (2017). Homeostatic Control
558 of Hpo/MST Kinase Activity through Autophosphorylation-Dependent Recruitment of the
559 STRIPAK PP2A Phosphatase Complex. Cell Rep *21*, 3612-3623.

560 Zheng, Y., and Pan, D. (2019). The Hippo Signaling Pathway in Development and Disease. Dev
561 Cell *50*, 264-282.

562 Zheng, Y., Wang, W., Liu, B., Deng, H., Uster, E., and Pan, D. (2015). Identification of
563 Happyhour/MAP4K as Alternative Hpo/Mst-like Kinases in the Hippo Kinase Cascade. Dev Cell
564 *34*, 642-655.
565

566

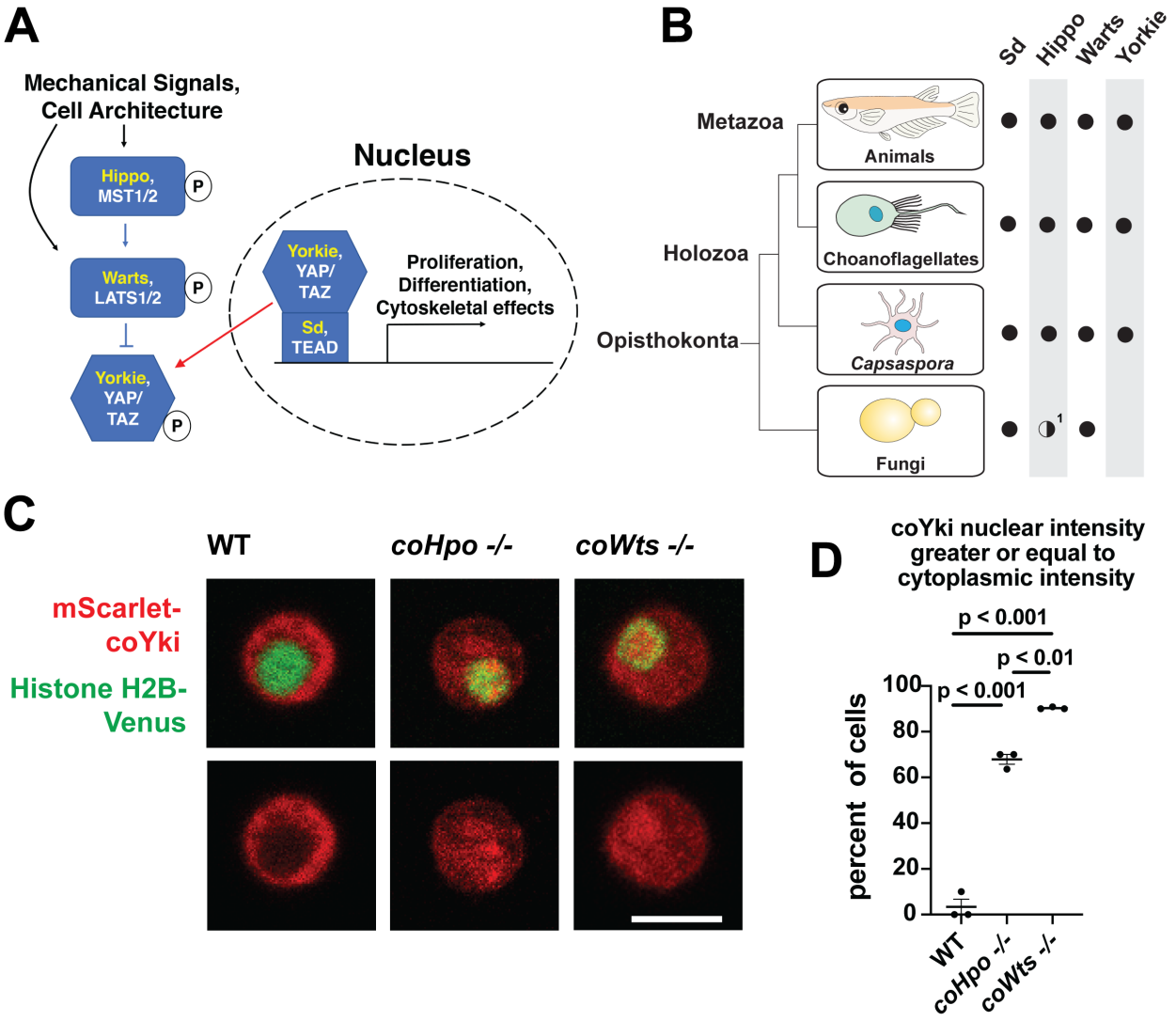

Figure 1. The Hippo pathway kinases regulate the subcellular localization of coYki. (A) The Hippo pathway in *Drosophila* (yellow text) and mammals (white text). Figure from (Phillips et al., 2022). **(B)** Conservation of Hippo pathway components in close unicellular relatives of animals. [1]The Hippo kinase SARAH domain is absent from putative Hippo kinase orthologs in yeasts, but is present in the early-branching fungus *Spizellomyces punctatus* and in amoebozoans such as *Dictyostelium*, indicating SARAH domain loss in some fungal lineages. Data from (Sebe-Pedros et al., 2012). **(C)** Cells were transiently transfected with the indicated constructs and imaged by confocal microscopy. Scale bar is 5 microns. **(D)** Intensity of mScarlet-coYki signal in the nucleus and cytoplasm of cells was quantified. Where p values are given, differences between conditions are significant (One-way ANOVA, Tukey's test, n = 3 with at least 10 cells measured for each independent experiment.) Values are mean ± SEM. Absence of error bars indicates that error is smaller than the plot symbol.

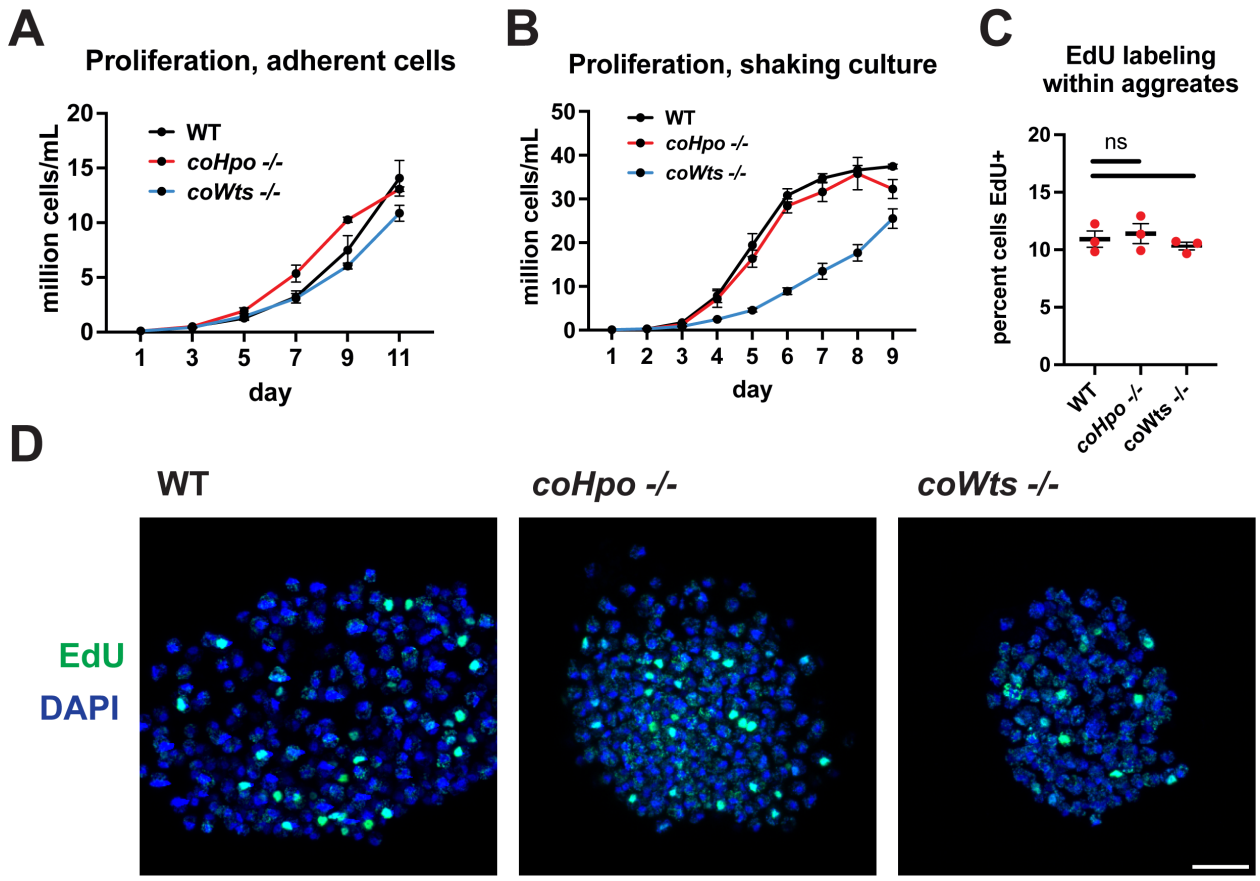

Figure 2. The Hippo pathway kinases do not restrict cell proliferation in *Capsaspora.* Cells were grown in adherent culture in 96-well plates **(A)** or in shaking culture **(B)** and cell density was measured daily by hemocytometer. **(C, D)** Cells were inoculated under low-adherence conditions to induce aggregate formation, and 3 days after induction aggregates were incubated with EdU for 4 hours, fixed, and processed to detect EdU labeling. Scale bar is 10 microns. Differences in EdU labeling between WT and mutants were not significant (one-way ANOVA, Dunnett's test, n = 3 with 3 aggregates measured for each independent experiment). Black bars show mean ± SEM, and red dots show values for individual aggregates.

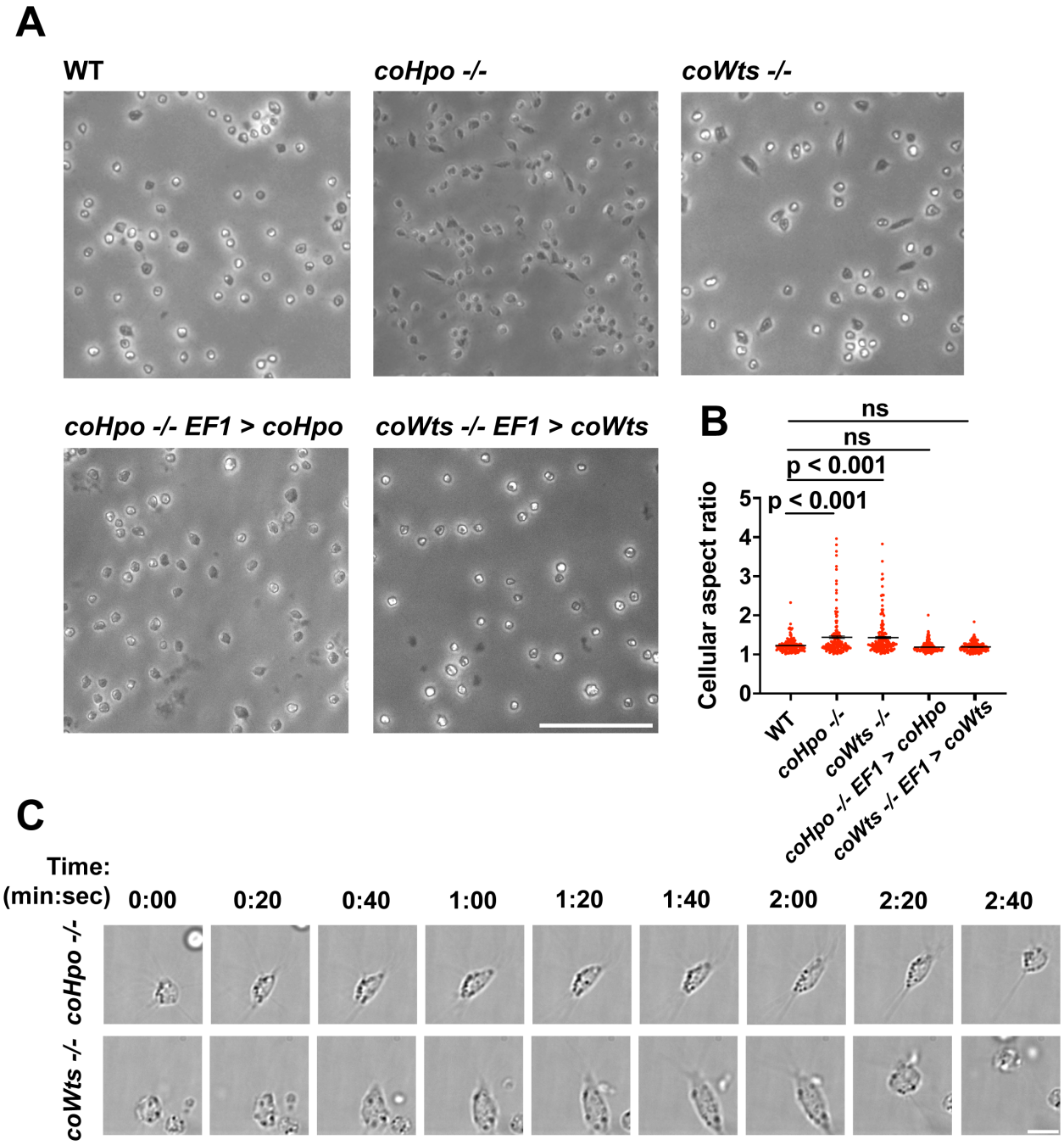

592

593 **Figure 3. The Hippo pathway kinases regulate cell morphology and a contractile cell**
594 **behavior in *Capsaspora*. (A)** Cells were inoculated into glass-bottom chamber slides, and
595 adherent cells were imaged two days after inoculation. Scale bar is 50 microns. **(B)** The aspect
596 ratio of cells imaged as described in (A) was measured using ImageJ. The differences between

597 WT and either *coHpo -/-* or *coWts -/-* cells are significant (one-way ANOVA, Dunnett's test, n = 3
598 with 50 cells measured for each independent experiment). Black bars show mean ± SEM, and
599 red dots show values for 150 individual cells. **(C)** Cells were prepared as described in (A) and
600 imaged by time lapse microscopy. Scale bar is 10 microns.
601
602

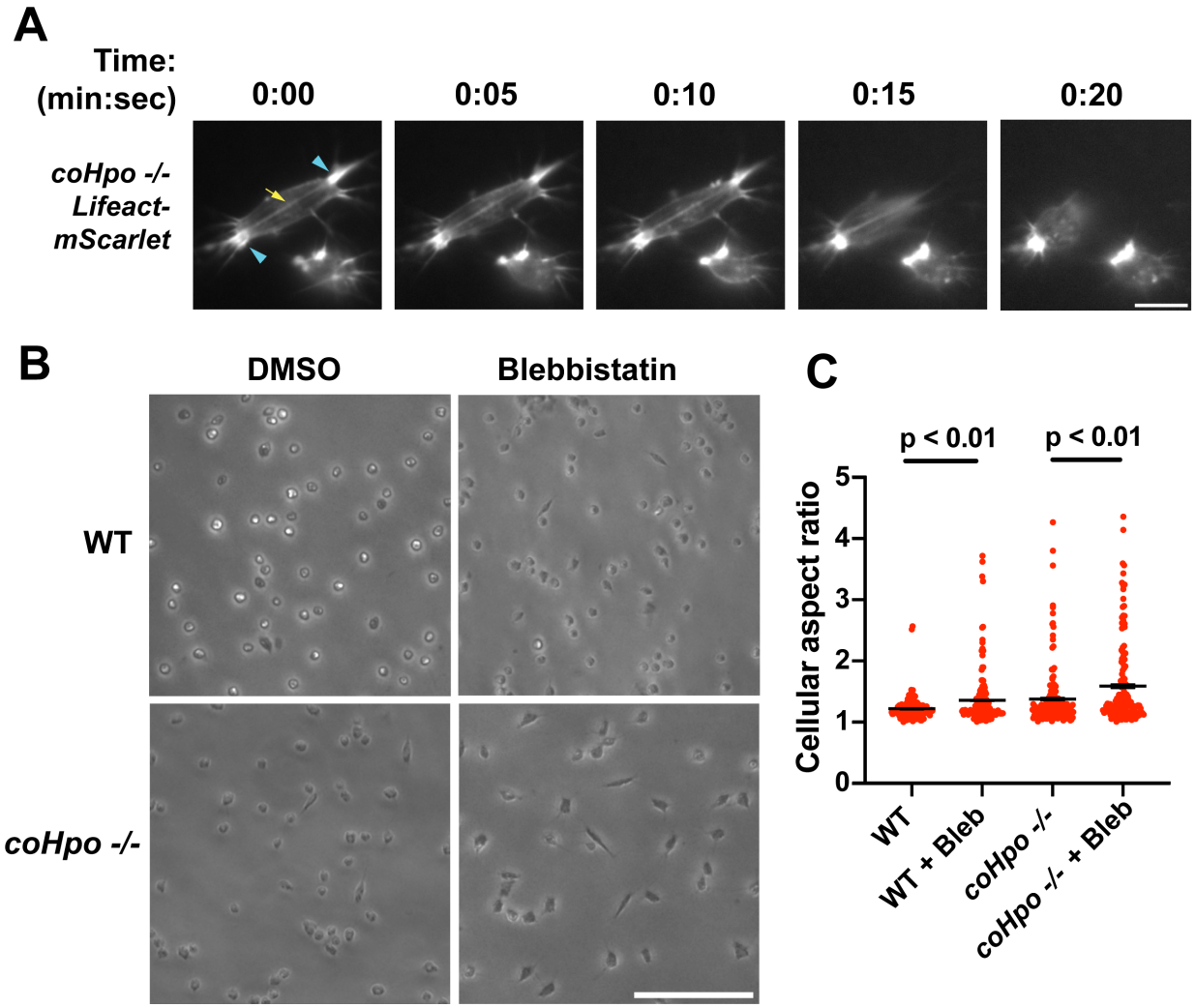

Figure 4. Characterization of actomyosin in contractile *Capsaspora* cells. (A) Cells were inoculated on glass-bottom chamber slides, and at 2 days after inoculation adherent cells were imaged by time-lapse epifluorescence microscopy. Blue arrowheads indicate ventral F-actin-enriched foci, and yellow arrow indicates the F-actin fiber that connects the foci. Scale bar is 10 microns. **(B)** Cells were inoculated on glass-bottom chamber slides. Two days after inoculation, DMSO or Blebbistatin at a concentration of 1 μM was added to cells. Cells were the imaged 24 hours after addition of blebbistatin. **(C)** The aspect ratio of cells prepared as in (B) was measured using ImageJ. For both WT and *coHpo -/-* cells, the difference between DMSO and blebbistatin treatment measurements are significant (t-test, n = 3 with 50 cells measured for each independent experiment). Black bars indicate mean ± SEM, and red dots indicate measurements for 150 individual cells for each condition. Absence of error bars indicates that error is smaller than the plot symbol.

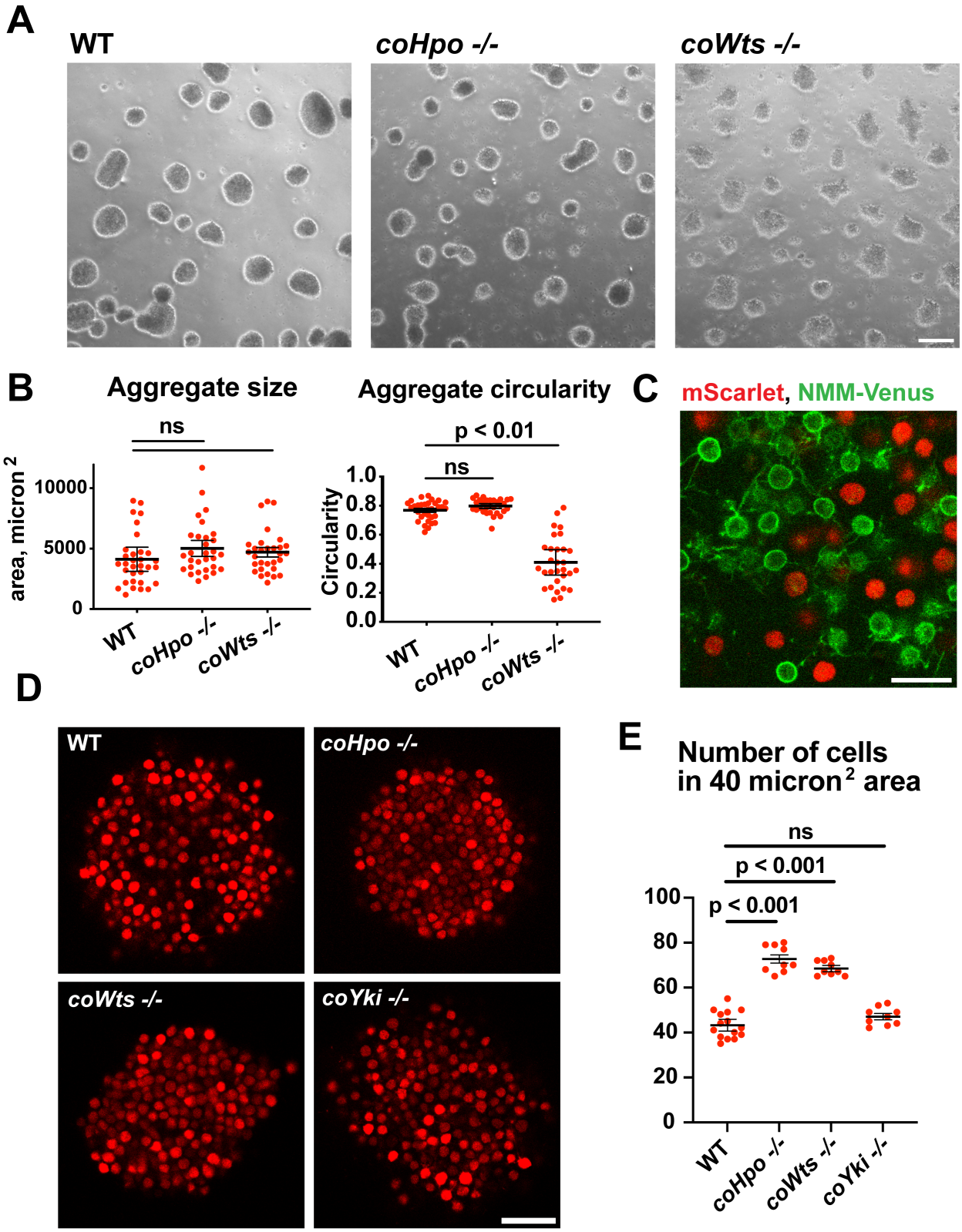

Figure 5. The Hippo pathway kinases regulate the density of cell packing in *Capsaspora* aggregates. (A) Aggregates were induced by inoculating cells in low-adherence conditions, and

aggregates were imaged at 5 days after inoculation. Scale bar is 100 microns. **(B)** the size and circularity of aggregates imaged as in (A) was measured using ImageJ. Black bars indicate mean ± SEM (n = 3 with 10 aggregates measured for each independent experiment), and red dots indicate values for 30 individual aggregates. For aggregate circularity, the difference between WT and *coWts -/-* aggregates is significant (one-way ANOVA, Dunnett's test.) **(C)** Cells expressing either mScarlet or N-myristoylation motif (NMM)-Venus, a marker of the plasma membrane which allows visualization of microvilli, were mixed 1:1 and inoculated into low-adherence conditions to induce aggregation. After 5 days, aggregates were imaged by confocal microscopy. Scale bar is 10 microns. **(D)** Clonal populations of cells of the indicated genotype stably expressing mScarlet were inoculated into low-adherence conditions, and cell aggregates were imaged 5 days after inoculation by confocal microscopy. Scale bar is 20 microns. **(E)** The number of cells within a 40 micron^2 area from aggregate optical sections imaged as in (D) was measured. Black bars indicate mean ± SEM (n = 3 with 3 aggregates measured for each independent experiment), and red dots indicate values for 9 individual aggregates for each condition. The difference between WT and either *coHpo -/-* or *coWts -/-* cells is significant (one-way ANOVA, Dunnett's test.)

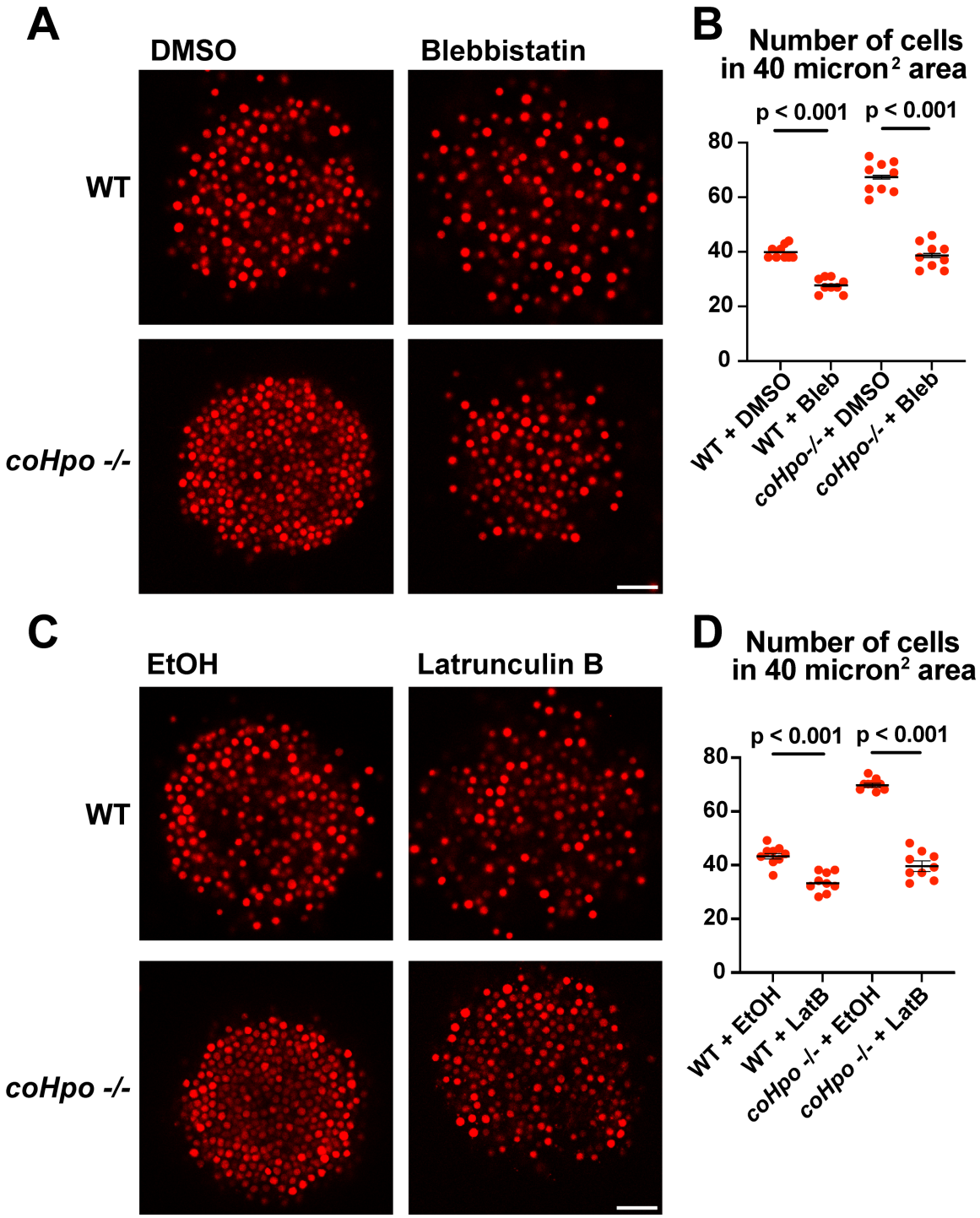

637

638

639 **Figure 6. Perturbation of the actomyosin network affects cell packing in multicellular**
640 ***Capsaspora* aggregates. (A)** Aggregates were treated with 20 μM blebbistatin or DMSO as a
641 vehicle control for 20 minutes and then imaged by confocal microscopy. Scale bar is 20 microns.
642 **(B)** Cells per area were quantified from images obtained as in (A). Black bars indicate means ±

643 SEM (n = 3 with 3 aggregates measured for each independent experiment), and red dots indicate
644 values for 9 individual aggregates for each condition. Absence of error bars indicates that error is
645 smaller than the plot symbol. For both WT and *coHpo -/-* aggregates, the difference between
646 DMSO and blebbistatin treatment is significant (t-test). **(C)** Aggregates were treated with 5 μg/ml
647 Latrunculin B or ethanol as a vehicle control for 1 hour and then imaged by confocal microscopy.
648 Scale bar is 20 microns. **(D)** Cells per area were quantified from images obtained as in (C). For
649 both WT and *coHpo -/-* aggregates, the difference between ethanol and Latrunculin B treatment
650 is significant (n = 3, t-test.)
651
652

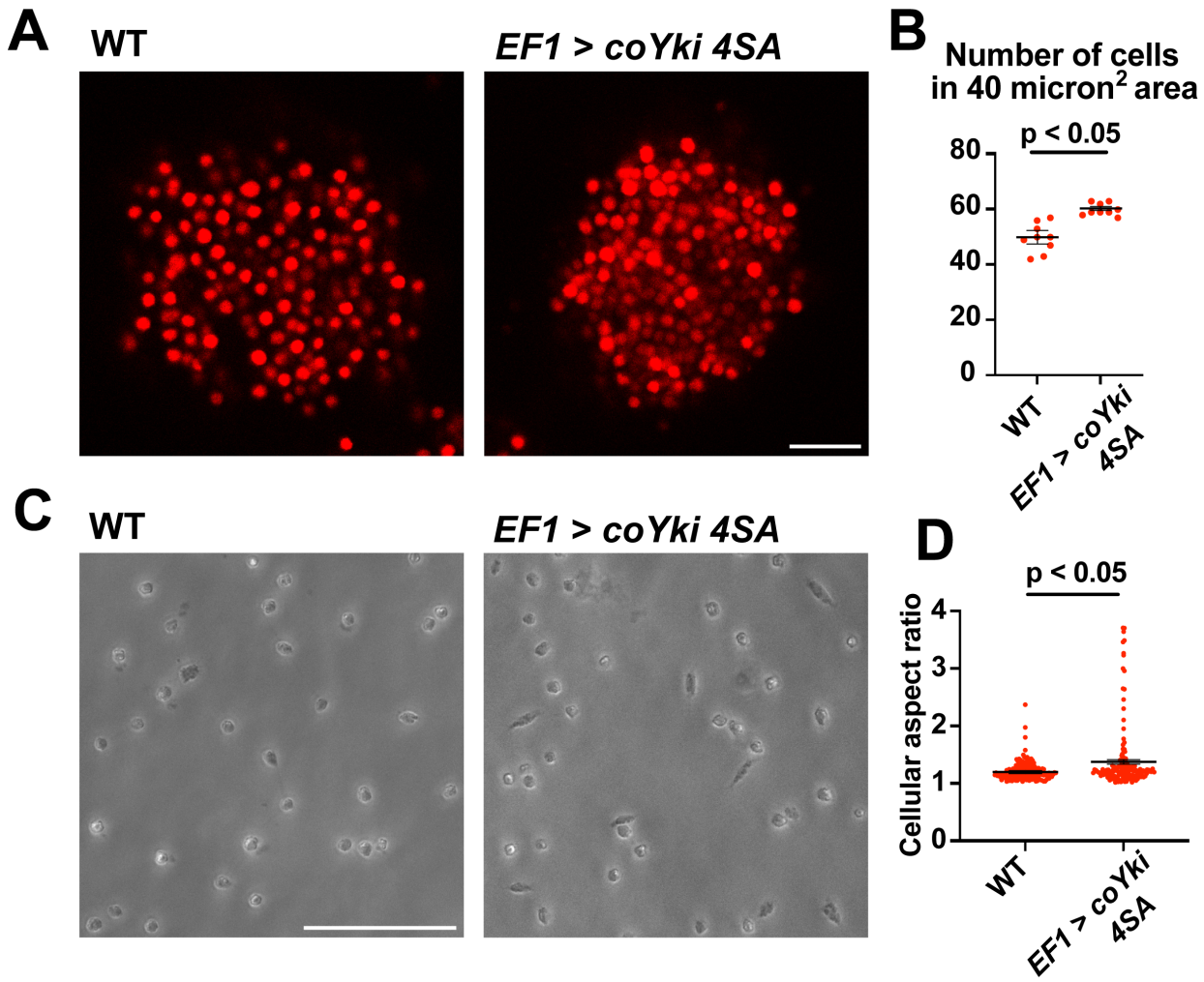

Figure 7. Expression of a constitutively active form of coYki phenocopies loss of *coHpo* or *coWts* in *Capsaspora*. (A) Aggregates were imaged 5 days after inoculation. Scale bar is 20 microns. **(B)** The number of cells within a 40 micron^2 area within an aggregate was measured. Black bars indicate mean ± SEM (n = 3 with 3 aggregates measured for each independent experiment), and red dots indicate values for 9 individual aggregates for each condition. The difference between WT and *EF1 > coYki 4SA* is significant (t-test). **(C)** Cells were inoculated into glass-bottom chamber slides and imaged 2 days after inoculation. Scale bar is 50 microns. **(D)** The aspect ratio of cells imaged as in (C) was measured using ImageJ. Black bars show mean ± SEM (n = 3 with 40 cells measured for each independent experiment), and red dots show values for 150 individual cells. The difference between WT and *EF1 > coYki 4SA* is significant (t-test).

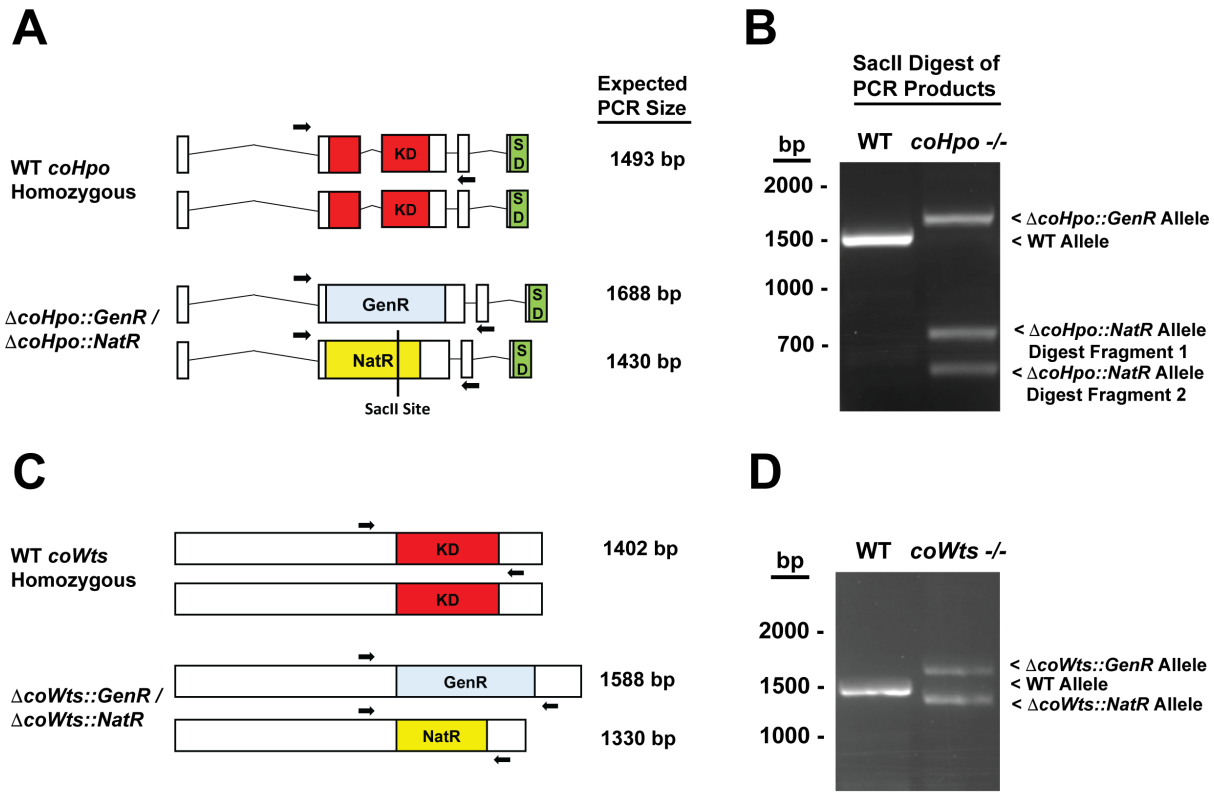

Figure 1- figure supplement 1. Knockout of *coHpo and coWts*. (A) A diagram of the *coHpo* genomic loci in WT or a putative *coHpo -/-* knockout line is shown. "KD" indicates kinase domain, "SD" indicates SARAH domain, "GenR" indicates a geneticin resistance cassette, and "NatR" indicates a nourseothricin resistance cassette. Arrows indicate a pair of primers used in PCR reactions. The same primer pair were used in all PCRs shown. Expected PCR product sizes for different alleles are given. A SacII site present only within the allele containing the NatR cassette is shown. **(B)** PCR products from WT and *coHpo -/-* cells using primers shown in (A). Because the product sizes for the WT and *ΔcoHpo::NatR* alleles are close in size, we digested PCR products with SacII, which uniquely cuts the *ΔcoHpo::NatR* allele. The *coHpo -/-* cell line shows the expected products for a homozygous knockout. Sequencing of PCR products confirmed the identity of the WT, *ΔcoHpo::GenR*, and *ΔcoHpo::NatR* alleles. **(C)** A diagram of the *coWts* genomic loci in WT or a putative *coWts -/-* knockout line is shown. "KD" indicates kinase domain, "GenR" indicates a geneticin resistance cassette, and "NatR" indicates a nourseothricin resistance cassette. Arrows indicate a pair of primers used in PCR reactions. The same primer pair were used in all PCRs shown. **(D)** PCR products from WT and *coHpo -/-* cells using primers

683 shown in (C). The *coWts -/-* cell line shows the expected products for a homozygous knockout.
684 Sequencing of PCR products confirmed the identity of the WT, *⊿coWts::GenR*, and *⊿coWts::NatR*
685 alleles.
686
687

688 **Video S1. Time-lapse microscopy of adherent WT *Capsaspora* cells.** This video serves as a
689 control for Videos S2 and S3.
690
691 **Video S2. Time-lapse microscopy of adherent *coHpo -/-* cells.**
692
693 **Video S3. Time-lapse microscopy of adherent *coWts -/-* cells.**
694
695 **Video S4. Time-lapse confocal microscopy of adherent WT cells expressing Lifeact-**
696 **mScarlet.** This video serves as a control for Video S5.
697
698 **Video S5. Time-lapse confocal microscopy of adherent *coHpo -/-* cells expressing Lifeact-**
699 **mScarlet.**
700

701 **Data S1. Sequences of synthesized gene fragments used in this study**

702

703

Figure 1-supplement 2-source data 1. Unedited gel image used to generate panel B.

Figure 1-supplement 2-source data 2. Uncropped annotated gel image used to generate panel B.

Figure 1-supplement 2-source data 3. Unedited gel image used to generate panel D.

Figure 1-supplement 2-source data 4. Uncropped annotated gel image used to generate panel D.